EGTRIB Journal
JOURNAL OF
THE EGYPTIAN SOCIETY OF TRIBOLOGY
VOLUME 19, No. 3, July 2022, pp. 80 - 93 **ISSN 2090 - 5882**
(Received June 21. 2022, Accepted in final form June 26. 2022) **jest.journals.ekb.eg**

Vibration of 2D FG Higher Order Plates using Differential Integral Quadrature Method

Amr E. Assie[1,2], Salwa Mohamed[3]

[1]Mechanical Engineering Department, Faculty of Engineering, Jazan University, P. O. Box 45142, Jazan, Kingdom of Saudi Arabia,

[2] Department of Mechanical Design and Production, Faculty of Engineering, Zagazig University, P.O. Box 44519, Zagazig, Egypt,

[3] Department of Engineering Mathematics, Faculty of Engineering, Zagazig University, P.O. Box 44519, Zagazig, Egypt.

ABSTRACT

This article presented a mathematical model to investigate the free vibration behavior of bi-directional (2D) functionally graded plate (FGP) using higher order shear deformation theory. The gradation of the material through the thickness and axial directions is described by power distribution function, which derived based on Voigt rule of mixture. Kinematic higher order shear theory developed by Reddy, equivalent single layer 2D constitutive equation, and Hamilton's principle are exploited to describe the strains, stress-strain relations, and equations of motions of 2D-FGP. Numerical differential integral quadrature method (DIQM) is manipulated to discretize the structure spatial domain and solve the system equations. Validation with previous work is presented. Numerical parametric studies are developed to illustrate the influence of gradation indices, slenderness ratio and aspect ratio on the natural frequencies of 2D-FG plate. The proposed model is economical in designing many applications used in nuclear, mechanical, aerospace, naval, dental, and medical fields.

KEYWORDS

Free vibration; Bi-directional FGM; Higher order Plate; Numerical DIQM.

INTRODUCTION

Functionally graded materials (FGM) which invented during the space-plane project in Japan 1984 [1], can be used as thermal barrier capable of withstanding a surface temperature of 2000 K and a temperature gradient of 1000 K across a cross-section <10 mm [2]. Nowadays, FGM can be used in many applications such as, aerospace, nuclear reactors, naval, electronics and biomedical structures.

Wu and Huang [3] developed a semi-analytical finite element method to evaluate the stress and deformation of 2D FG truncated conical shells. Abo-Bakr et al. [4,5] evaluated the

optimum weight of FG microbeam under the buckling and free vibrations constraints using multiobjective shape optimization. Yu et al. [6] studied the buckling and free vibration of laminated composites plates with cutouts by using a new simple first order shear deformation with 4 variables. Nguyen et al. [7] investigated analytically the bending and vibration of FG plates based on a refined simple first-order shear deformation theory. Based on quasi-3D higher shear deformation theory with five unknowns (HSDT), Khiloun et al. [8] developed an analytical solution to study a bending and vibration of thick advanced composite plates using a four-variable quasi 3D HSDT. Arshid et al. [9] examined a vibration of FG porous modified couple stress microplates under hygrothermal effect. Pham et al. [10] exploited finite element method and a quasi-3D nonlocal theory to analysis the vibration of FGM nanoplates rested on elastic foundations in the thermal environment. Attia and Shanab [11,12] studied the bending, buckling, and vibration characteristics of 2D FGM nanobeams with couple stress and surface energy using Navier analytical solution. Hendi et al. [13] studied nonlinear thermal vibration of pre/post-buckled two-dimensional FGM tapered microbeams based higher deformation theory. Ohab-Yazdi et al. [14] studied the vibration of 2D-FG rotary nonlocal nanobeam with even porosity distribution by generalized differential quadrature method (GDQM).

Van [15] exploited hybrid quasi-3D plate theory to study the bending and vibration of 2D FGM sandwich plate laid on Pasternak's elastic foundations. Sadgui and Tati [16] used a trigonometric shear deformation theory in analyzing of buckling and free vibration of FG plates. Tran et al. [17] studied the vibration of FG plates resting on the elastic foundation in the thermal environment by using first order shear deformation theory. Civalek and Avcar [18] analyzed buckling and vibration response of CNT reinforced laminated non-rectangular plates by discrete singular convolution method. Barati et al. [19] studied the vibration 2D FG nonlocal nanobeams under magnetic field using generalized differential quadrature method. Babaei et al. [20] studied the static and vibration responses of FG porous annular elliptical sector plate based on 3D finite element method, where the porosity defined by nonlinear symmetric, nonsymmetric and uniform functions. Katiyar and Gupta [21] investigated the vibration of FG porous plate rested on elastic foundation and subjected to thermal influence by using refined non-polynomial trigonometric higher-order shear deformation theory. Sah and Ghosh [22] studied free vibration and buckling of multi-directional FG sandwich plates with porosity using even and uneven functional distributions.

Based on the previous works and literature survey, the free vibration behaviors of bidirectional FG plate modelled by higher order shear deformation plate theory has not been addressed. Therefore, this article aims to present this topic in comprehensive analysis. The rest of the article is organized as following: - the problem formulation including the kinematic displacement filed, constitutive relations, equations of motion, and boundary conditions are developed in section 2. Section 3 presents a solution methodology and a discretization of spatial coordinates. Model validations numerical results, and parametric studies are discussed through section 4. Conclusions and main features are summarized in section 5.

PROBLEM FORMULATION

The displacement field based on high-order shear deformation theory with no shear correction factors can be expressed as

$(x, y, z) = u_o(x, y) - z\frac{\partial w_b}{\partial x} - F(z)\frac{\partial w_s}{\partial x}$	**(1)**
$v(x, y, z) = v_o(x, y) - z\frac{\partial w_b}{\partial y} - F(z)\frac{\partial w_s}{\partial y}$	**(2)**
$w(x, y, z) = w_b(x, y) + w_s(x, y)$	**(3)**

In which

$F(z) = \frac{4z^3}{3h^2}$	**(4)**

where: u_o , v_o , w_b and w_s are the displacements defined at the midplane. w_b and w_s stand for bending and shear parts, respectively. $F(z)$ is a shape function that estimates the distribution of transverse shear.

The normal and shear strains associated with the displacement field portrayed by

$\varepsilon_x = \varepsilon_x^0 - z\frac{\partial^2 w_b}{\partial x^2} - F(z)\frac{\partial^2 w_s}{\partial x^2}$	**(5)**
$\varepsilon_y = \varepsilon_y^0 - z\frac{\partial^2 w_b}{\partial y^2} - F(z)\frac{\partial^2 w_s}{\partial y^2}$	**(6)**
$\gamma_{xy} = \gamma_{xy}^0 - z\left(2\frac{\partial^2 w_b}{\partial x \partial y}\right) - F(z)\left(2\frac{\partial^2 w_s}{\partial x \partial y}\right)$	**(7)**
$\gamma_{yz} = G(z)\frac{\partial w_s}{\partial y}$	**(8)**
$\gamma_{xz} = G(z)\frac{\partial w_s}{\partial x}$	**(9)**

where

$\varepsilon_x^o = \frac{\partial u_o}{\partial x}, \ \varepsilon_y^o = \frac{\partial v_o}{\partial y} \quad and \ \gamma_{xy}^o = \frac{\partial u_o}{\partial y} + \frac{\partial v_o}{\partial x}$	**(10)**
$F(z) = z - f(z) \qquad \& \quad G(z) = 1 - F'(z) = f'(z)$	**(11)**

The stress-strain constitutive relations (plane stress) for 2D shear deformation plate theory $(\varepsilon_z = 0)$ under isothermal conditions can be defined by

$\begin{bmatrix} \sigma_x \\ \sigma_y \\ \tau_{xy} \\ \tau_{yz} \\ \tau_{xz} \end{bmatrix} = \begin{bmatrix} Q_{11} & Q_{12} & 0 & 0 & 0 \\ Q_{12} & Q_{22} & 0 & 0 & 0 \\ 0 & 0 & Q_{66} & 0 & 0 \\ 0 & 0 & 0 & Q_{44} & 0 \\ 0 & 0 & 0 & 0 & Q_{55} \end{bmatrix} \begin{bmatrix} \varepsilon_x \\ \varepsilon_y \\ \gamma_{xy} \\ \gamma_{yz} \\ \gamma_{xz} \end{bmatrix}$	**(12)**

For isotropic materials, the plane stress stiffnesses are:

$$Q_{11} = Q_{22} = \frac{E}{1-v^2}, \qquad Q_{12} = \frac{vE}{1-v^2},$$ $$Q_{44} = Q_{55} = Q_{66} = \frac{E}{2(1+v)}$$	**(13)**

Where E is the Young modulus and ν is the Poisson's ratio. By assuming that, the FG material properties are graded in both axial directions (x -axis) and transverse directions (z -axis) according to power law as

$$P(x,z,\phi) = [P_m + P_{cm}\left(\frac{1}{2}+\frac{z}{h}\right)^{n_z}(\frac{x}{a})^{n_x}]$$ $$P_{cm} = P_c - P_m$$	**(14)**

The governing equations of equilibrium and associated boundary conditions of the developed model are derived using Hamilton's Principles.

$$\int_0^T \delta(U+V-K)dt = 0$$	**(15)**

The virtual potential work of applied in-plane loads can be expressed in the form, δV:-

$$\delta V = \int_A \left(N_x^o \frac{\partial \bar{w}}{\partial x}\frac{\partial \delta \bar{w}}{\partial x} + N_{xy}^o\left(\frac{\partial \bar{w}}{\partial x}\frac{\partial \delta \bar{w}}{\partial y} + \frac{\partial \bar{w}}{\partial y}\frac{\partial \delta \bar{w}}{\partial x}\right) + N_y^o \frac{\partial \bar{w}}{\partial y}\frac{\partial \delta \bar{w}}{\partial y}\right) dA$$	**(16)**

The variation, δV using Hamilton's Principles results in the following

$$\bar{N}^o = N_x^o \frac{\partial^2 \bar{w}}{\partial x^2} + 2\,N_{xy}^o \frac{\partial^2 \bar{w}}{\partial x \partial y} + N_y^o \frac{\partial^2 \bar{w}}{\partial y^2}$$	**(17)**

The virtual Kinetic Energy δK:

$$\delta K = \int_V \rho(x,z,\phi)[\dot{u}\delta\dot{u} + \dot{v}\delta\dot{v} + \dot{w}\delta\dot{w}]\, dV$$ $$\delta K = \int_A \Big[\mathrm{I}_o(x)\big(\dot{u}_o\delta\dot{u}_o + \dot{v}_o\delta\dot{v}_o + (\dot{w}_b + \dot{w}_s)\delta(\dot{w}_b + \dot{w}_s)\big) - \mathrm{I}_1(x)\left(\dot{u}_o\frac{\partial\delta\dot{w}_s}{\partial x} + \frac{\partial\dot{w}_s}{\partial x}\delta\dot{u}_o + \dot{v}_o\frac{\partial\delta\dot{w}_b}{\partial y} + \frac{\partial\dot{w}_b}{\partial y}\delta\dot{v}_o\right) - \mathrm{J}_1(x)\left(\dot{u}_o\frac{\partial\delta\dot{w}_s}{\partial x} + \frac{\partial\dot{w}_s}{\partial x}\delta\dot{u}_o + \dot{v}_o\frac{\partial\delta\dot{w}_b}{\partial y} + \frac{\partial\dot{w}_b}{\partial y}\delta\dot{v}_o\right) +$$	**(18)**

$\mathbf{I}_2(x)\left(\frac{\partial \dot{w}_b}{\partial x}\frac{\partial \delta \dot{w}_b}{\partial x}+\frac{\partial \dot{w}_b}{\partial y}\frac{\partial \delta \dot{w}_b}{\partial y}\right)+\mathbf{J}_2(x)\left(\frac{\partial \dot{w}_b}{\partial x}\frac{\partial \delta \dot{w}_s}{\partial x}+\frac{\partial \dot{w}_s}{\partial x}\frac{\partial \delta \dot{w}_b}{\partial x}+\frac{\partial \dot{w}_b}{\partial y}\frac{\partial \delta \dot{w}_s}{\partial y}+\frac{\partial \dot{w}_s}{\partial y}\frac{\partial \delta \dot{w}_b}{\partial y}\right)+\mathbf{K}_2(x)\left(\frac{\partial \dot{w}_s}{\partial x}\frac{\partial \delta \dot{w}_s}{\partial x}+\frac{\partial \dot{w}_s}{\partial y}\frac{\partial \delta \dot{w}_s}{\partial y}\right)\Big]\,dA$	

The virtual strain energy δU:

$\delta U=\int_V\left(\sigma_x\delta\varepsilon_x+\sigma_y\delta\varepsilon_y+\tau_{xy}\delta\gamma_{xy}+\tau_{xz}\delta\gamma_{xz}+\tau_{yz}\delta\gamma_{yz}\right)dV$ $\delta U=\int_A\Big[N_x\delta\varepsilon_x^0+N_y\delta\varepsilon_y^0+N_{xy}\delta\gamma_{xy}^0-M_x^b\frac{\partial^2\delta w_b}{\partial x^2}-M_y^b\frac{\partial^2\delta w_b}{\partial y^2}-M_{xy}^b\left(2\frac{\partial^2\delta w_b}{\partial x\partial y}\right)-M_x^s\frac{\partial^2\delta w_s}{\partial x^2}-M_y^s\frac{\partial^2\delta w_s}{\partial y^2}-M_{xy}^s\left(2\frac{\partial^2\delta w_s}{\partial x\partial y}\right)+S_{yz}^s\frac{\partial\delta w_s}{\partial y}+S_{xz}^s\frac{\partial\delta w_s}{\partial x}\Big]\,dA$	**(19)**

Substituting Eqns. (16), (18) and (19) for $\delta V, \delta K$ and δU, respectively into Eq. (15) and performing integration by parts, the equations of FGM plate in terms of displacements can be represented by

$A_{11}(x)\frac{\partial^2u_o}{\partial x^2}+\left(A_{12}(x)+A_{66}(x)\right)\frac{\partial^2v_o}{\partial x\partial y}+A_{66}(x)\frac{\partial^2u_o}{\partial y^2}+A'_{11}(x)\frac{\partial u_o}{\partial x}+A'_{12}(x)\frac{\partial v_o}{\partial y}-\left(B_{12}(x)+2B_{66}(x)\right)\frac{\partial^3w_b}{\partial x\partial y^2}-\left(B^s_{12}(x)+2B^s{}_{66}(x)\right)\frac{\partial^3w_s}{\partial x\partial y^2}-B_{11}(x)\frac{\partial^3w_b}{\partial x^3}-B^s_{11}(x)\frac{\partial^3w_s}{\partial x^3}-B'_{11}(x)\frac{\partial^2w_b}{\partial x^2}-B'_{12}(x)\frac{\partial^2w_b}{\partial y^2}-B^{s'}_{11}(x)\frac{\partial^2w_s}{\partial x^2}-B^{s'}_{12}(x)\frac{\partial^2w_s}{\partial y^2}=I_o(x)\ddot{u}_o-I_1(x)\frac{\partial\ddot{w}_b}{\partial x}-J_1(x)\frac{\partial\ddot{w}_s}{\partial x}$	**(20)**
$A_{22}(x)\frac{\partial^2v_o}{\partial y^2}+\left(A_{12}(x)+A_{66}(x)\right)\frac{\partial^2u_o}{\partial x\partial y}+A_{66}(x)\frac{\partial^2v_o}{\partial x^2}+A'_{66}(x)\left(\frac{\partial u_o}{\partial y}+\frac{\partial v_o}{\partial x}\right)-\left(B_{12}(x)+2B_{66}(x)\right)\frac{\partial^3w_b}{\partial x^2\partial y}-\left(B^s_{12}(x)+2B^s_{66}(x)\right)\frac{\partial^3w_s}{\partial x^2\partial y}-B_{22}(x)\frac{\partial^3w_b}{\partial y^3}-B^s_{22}(x)\frac{\partial^3w_s}{\partial y^3}-2B'_{66}(x)\frac{\partial^2w_b}{\partial x\partial y}-2B^{s'}_{66}(x)\frac{\partial^2w_s}{\partial x\partial y}=I_o(x)\ddot{v}_o-I_1(x)\frac{\partial\ddot{w}_b}{\partial y}-J_1(x)\frac{\partial\ddot{w}_s}{\partial y}$	**(21)**
$B_{11}(x)\frac{\partial^3u_o}{\partial x^3}+B_{22}(x)\frac{\partial^3v_o}{\partial y^3}+\left(B_{12}(x)+2B_{66}(x)\right)\left(\frac{\partial^3u_o}{\partial x\partial y^2}+\frac{\partial^3v_o}{\partial x^2\partial y}\right)+2\left(B'_{12}(x)+B'_{66}(x)\right)\frac{\partial^2v_o}{\partial x\partial y}+2B'_{66}(x)\frac{\partial^2u_o}{\partial y^2}+2B'_{11}(x)\frac{\partial^2u_o}{\partial x^2}+B''_{11}(x)\frac{\partial u_o}{\partial x}+B''_{12}(x)\frac{\partial v_o}{\partial y}-D_{11}(x)\frac{\partial^4w_b}{\partial x^4}-D_{22}(x)\frac{\partial^4w_b}{\partial y^4}-D^s_{11}(x)\frac{\partial^4w_s}{\partial x^4}-D^s_{22}(x)\frac{\partial^4w_s}{\partial y^4}-2\left(D_{12}(x)+2D_{66}(x)\right)\frac{\partial^4w_b}{\partial x^2\partial y^2}-2\left(D^s_{12}(x)+2D^s_{66}(x)\right)\frac{\partial^4w_s}{\partial x^2\partial y^2}-2\left(D'_{12}(x)+\right.$	**(22)**

$2D'_{66}(x)\big)\frac{\partial^3 w_b}{\partial x\partial y^2} - 2\left(D^{s'}_{12}(x) + 2D^{s'}_{66}(x)\right)\frac{\partial^3 w_s}{\partial x\partial y^2} - 2D'_{11}(x)\frac{\partial^3 w_b}{\partial x^3} - 2D^{s'}_{11}(x)\frac{\partial^3 w_s}{\partial x^3} - D''_{11}(x)\frac{\partial^2 w_b}{\partial x^2} - D^{s''}_{11}(x)\frac{\partial^2 w_s}{\partial x^2} - D''_{12}(x)\frac{\partial^2 w_b}{\partial y^2} - D^{s''}_{12}(x)\frac{\partial^2 w_s}{\partial y^2} + \bar{N}^o = I_o(x)(\ddot{w}_b + \ddot{w}_s) + I'_1(x)\ddot{u}_o + I_1(x)(\frac{\partial \ddot{u}_o}{\partial x} + \frac{\partial \ddot{v}_o}{\partial y}) - I'_2(x)\frac{\partial \ddot{w}_b}{\partial x} - I_2(x)\nabla^2\ddot{w}_b - J'_2(x)\frac{\partial \ddot{w}_s}{\partial x} - J_2(x)\nabla^2\ddot{w}_s$	
$B^s_{11}(x)\frac{\partial^3 u_o}{\partial x^3} + B^s_{22}(x)\frac{\partial^3 v_o}{\partial y^3} + \left(B^s_{12}(x) + 2B^s_{66}(x)\right)\left(\frac{\partial^3 u_o}{\partial x\partial y^2} + \frac{\partial^3 v_o}{\partial x^2\partial y}\right) + 2\left(B^{s'}_{12}(x) + B^{s'}_{66}(x)\right)\frac{\partial^2 v_o}{\partial x\partial y} + 2B^{s'}_{66}(x)\frac{\partial^2 u_o}{\partial y^2} + 2B^{s'}_{11}(x)\frac{\partial^2 u_o}{\partial x^2} + B^{s''}_{11}(x)\frac{\partial u_o}{\partial x} + B^{s''}_{12}(x)\frac{\partial v_o}{\partial y} - D^s_{11}(x)\frac{\partial^4 w_b}{\partial x^4} - D^s_{22}(x)\frac{\partial^4 w_b}{\partial y^4} - H^s_{11}(x)\frac{\partial^4 w_s}{\partial x^4} - H^s_{22}(x)\frac{\partial^4 w_s}{\partial y^4} - 2\big(D^s_{12}(x) + 2D^s_{66}(x)\big)\frac{\partial^4 w_b}{\partial x^2\partial y^2} - 2(H^s_{12}(x) + 2H^s_{66}(x)\frac{\partial^4 w_s}{\partial x^2\partial y^2} - 2\left(D^{s'}_{12}(x) + 2D^{s'}_{66}(x)\right)\frac{\partial^3 w_b}{\partial x\partial y^2} - 2\left(H^{s'}_{12}(x) + 2H^{s'}_{66}(x)\right)\frac{\partial^3 w_s}{\partial x\partial y^2} - 2\,D^{s'}_{11}(x)\frac{\partial^3 w_b}{\partial x^3} - H^{s'}_{11}(x)\frac{\partial^3 w_s}{\partial x^3} - D^{s''}_{11}(x)\frac{\partial^2 w_b}{\partial x^2} - D^{s''}_{12}(x)\frac{\partial^2 w_b}{\partial y^2} - H^{s''}_{11}(x)\frac{\partial^2 w_s}{\partial x^2} - H^{s''}_{12}(x)\frac{\partial^2 w_s}{\partial y^2} + A^s_{44}(x)\frac{\partial^2 w_s}{\partial y^2} + A^s_{55}(x)\frac{\partial^2 w_s}{\partial x^2} + A^{s'}_{55}\frac{\partial w_s}{\partial x} + \bar{N}^o = I_o(x)(\ddot{w}_b + \ddot{w}_s) + J'_1(x)\ddot{u}_o + J_1(x)(\frac{\partial \ddot{u}_o}{\partial x} + \frac{\partial \ddot{v}_o}{\partial y}) - J'_2(x)\frac{\partial \ddot{w}_b}{\partial x} - J_2(x)\nabla^2\ddot{w}_b - K'_2(x)\frac{\partial \ddot{w}_s}{\partial x} - K_2(x)\nabla^2\ddot{w}_s$	**(23)**

where: Rigidities and Inertia terms are obtained as functions of x as: -

$(A_{ij}(x), B_{ij}(x), D_{ij}(x), B^s_{ij}(x), D^s_{ij}(x), H^s_{ij}(x)) = \int_{-h/2}^{h/2} Q_{ij}(x,z) * [1, z, z^2, F(z), zF(z), (F(z))^2]dz$ $ij = 11, 12, 22, 66$	**(24)**
$A^s_{ij}(x) = \int_{-h/2}^{h/2} Q_{ij}(x,z)(G(z))^2 dz, \quad ij = 44, 55$	**(25)**
$(I_o(x), I_1(x), I_2(x)) = \int_{-h/2}^{h/2} \rho(x,z,\phi)(1, z, z^2)dz$	**(27)**
$(J_1(x), J_2(x), K_2(x)) =$ $\int_{-h/2}^{h/2} \rho(x,z,\phi)(F(z), zF(z), (F(z))^2)dz$	**(28)**

To have the nontrivial solutions (Eigen frequencies, ω_i) for the free vibration analysis, it is essential to ignore the in-plane forces, $\bar{N}^o$ in Eqns. (20-23).

The used boundary conditions: -

Clamped edge: $w_b, w_s, u_{\bar{n}}, u_{\bar{s}}, \frac{\partial w_b}{\partial \bar{n}}, \frac{\partial w_s}{\partial \bar{n}}, \frac{\partial w_b}{\partial \bar{s}},$

Simply supported edge: $w_b, w_s, u_{\bar{s}}, N_{\bar{n}\bar{n}}, M^b_{\bar{n}\bar{n}}, M^s_{\bar{n}\bar{n}}$

SOLUTION METHODOLOGY

Consider a partial differential equation in the unknown function $\theta(x, y)$. The two-dimensional domain of the independent variables $0 < x < a$, $0 < y < b$ is discretized by $n-$ and $m-$points, respectively. However, the objective of the discretization process is to transform the partial differential equation into an algebraic system in an unknown vector θ consisting of all discrete values of the unknown function. For this purpose, the unknowns $\theta_{ij} = \theta(x_j, y_i), i = 1, \cdots, m, j = 1, \cdots, n$ defined on the rectangular domain are rearranged vector after vector to form the whole unknown vector

$\theta = [\theta_{11}, \cdots \theta_{m1}, \theta_{12}, \cdots \theta_{m2}, \cdots \cdots \theta_{mn}]^T$	**(29)**

Let D_x be the first order derivative matrix with respect to x of dimension $n \times n$ and let D_y be the first order derivative matrix with respect to y of dimension $m \times m$. To be consistent with the arrangement of unknowns given in Eq. (29) for vector θ, the Kronecker product is used to construct global derivative matrices of dimension $(mn \times mn)$ as

$\begin{Bmatrix} \mathbb{D}_x \\ \mathbb{D}_y \end{Bmatrix} = \begin{Bmatrix} D_x \otimes I_m \\ I_n \otimes D_y \end{Bmatrix}$	**(30)**

where I_n and I_m are the identity matrices of dimensions $(n \times n)$ and $(m \times m)$, respectively and $'\otimes'$ denotes the Kronecker product. Based on Eq. (30), DQM can approximate higher and mixed partial derivatives such as $\partial^2\theta/\partial x^2$, $\partial^2\theta/\partial y^2$, $\partial^2\theta/\partial x \partial y$ by $\mathbb{D}_{xx}\theta, \mathbb{D}_{yy}\theta$ and $\mathbb{D}_{xy}\theta$, respectively, where $\mathbb{D}_{xx} = \mathbb{D}_x^2$, $\mathbb{D}_{yy} = \mathbb{D}_y^2$, and $\mathbb{D}_{xy} = \mathbb{D}_x\mathbb{D}_y$.

Now, since the mathematical model for the unified BDFG plate consists of four equations in the unknown functions $u_0(x, y), v_0(x, y), w_b(x, y)$ and $w_s(x, y)$, the overall discretized unknown vector is defined by $X = [U^T, V^T, W_b^T, W_s^T]^T$ where each of U, V, W_b, W_s is $(nm \times 1)$-vector. With respect to the kinetic terms in Eqs. (20-23), the following equations of motion for free vibration can be evaluated as

$(\mathcal{K} - \omega^2 \mathcal{M})X = 0$	**(31)**

Where

$$\mathcal{M} = \begin{bmatrix} \boldsymbol{I_0} \circ \mathbb{I} & \mathbb{O} & -\boldsymbol{I_1} \circ \mathbb{D}_x & -\boldsymbol{J_1} \circ \mathbb{D}_x \\ \mathbb{O} & I_0 \circ \mathbb{I} & -\boldsymbol{I_1} \circ \mathbb{D}_y & -\boldsymbol{J_1} \circ \mathbb{D}_y \\ (\mathbb{D}_x \boldsymbol{I_1}) \circ \mathbb{I} + \boldsymbol{I_1} \circ \mathbb{D}_x & \boldsymbol{I_1} \circ \mathbb{D}_y & \boldsymbol{I_0} \circ \mathbb{I} - (\mathbb{D}_x \boldsymbol{I_2}) \circ \mathbb{D}_x - \boldsymbol{I_2} \circ (\mathbb{D}_{xx} + \mathbb{D}_{yy}) & \boldsymbol{I_0} \circ \mathbb{I} - (\mathbb{D}_x \boldsymbol{J_2}) \circ \mathbb{D}_x - \boldsymbol{J_2} \circ (\mathbb{D}_{xx} + \mathbb{D}_{yy}) \\ (\mathbb{D}_x \boldsymbol{J_1}) \circ \mathbb{I} + \boldsymbol{J_1} \circ \mathbb{D}_x & \boldsymbol{J_1} \circ \mathbb{D}_y & \boldsymbol{I_0} \circ \mathbb{I} - (\mathbb{D}_x \boldsymbol{J_2}) \circ \mathbb{D}_x - \boldsymbol{J_2} \circ (\mathbb{D}_{xx} + \mathbb{D}_{yy}) & \boldsymbol{I_0} \circ \mathbb{I} - (\mathbb{D}_x \boldsymbol{K_2}) \circ \mathbb{D}_x - \boldsymbol{K_2} \circ (\mathbb{D}_{xx} + \mathbb{D}_{yy}) \end{bmatrix} \quad \textbf{(32)}$$

and

$$\begin{aligned}
K_{11} &= \mathbb{D}x(\boldsymbol{\mathcal{A}}_{11} \circ \mathbb{D}_x) + \mathbb{D}y(\boldsymbol{\mathcal{A}}_{66} \circ \mathbb{D}_y) \\
K_{12} &= \mathbb{D}x(\ \boldsymbol{\mathcal{A}}_{12} \circ \mathbb{D}_y) + \mathbb{D}y(\boldsymbol{\mathcal{A}}_{66} \circ \mathbb{D}_x) \\
K_{13} &= -\mathbb{D}x(\boldsymbol{\mathcal{B}}_{11} \circ \mathbb{D}_{xx} + \boldsymbol{\mathcal{B}}_{12} \circ \mathbb{D}_{yy}) - \mathbb{D}y(2\boldsymbol{\mathcal{B}}_{66} \circ \mathbb{D}_{xy}) \\
K_{14} &= -\mathbb{D}x(\boldsymbol{\mathcal{B}}^s_{11} \circ \mathbb{D}_{xx} + \boldsymbol{\mathcal{B}}^s_{12} \circ \mathbb{D}_{yy}) - \mathbb{D}y(2\boldsymbol{\mathcal{B}}^s_{66} \circ \mathbb{D}_{xy}) \\
K_{21} &= \mathbb{D}x(\boldsymbol{\mathcal{A}}_{66} \circ \mathbb{D}_y) + \mathbb{D}y(\boldsymbol{\mathcal{A}}_{12} \circ \mathbb{D}_x) \\
K_{22} &= \mathbb{D}x(\boldsymbol{\mathcal{A}}_{66} \circ \mathbb{D}_x) + \mathbb{D}y(\boldsymbol{\mathcal{A}}_{22} \circ \mathbb{D}_y) \\
K_{23} &= -\mathbb{D}x(2\boldsymbol{\mathcal{B}}_{66} \circ \mathbb{D}_{xy}) - \mathbb{D}y(\boldsymbol{\mathcal{B}}_{12} \circ \mathbb{D}_{xx} + \boldsymbol{\mathcal{B}}_{22} \circ \mathbb{D}_{yy}) \\
K_{24} &= -\mathbb{D}x(2\boldsymbol{\mathcal{B}}^s_{66} \circ \mathbb{D}_{xy}) - \mathbb{D}y(\boldsymbol{\mathcal{B}}^s_{12} \circ \mathbb{D}_{xx} + \boldsymbol{\mathcal{B}}^s_{22} \circ \mathbb{D}_{yy}) \\
K_{31} &= \mathbb{D}xx(\boldsymbol{\mathcal{B}}_{11} \circ \mathbb{D}_x) + 2\mathbb{D}xy(\boldsymbol{\mathcal{B}}_{66} \circ \mathbb{D}_y) + \mathbb{D}yy(\boldsymbol{\mathcal{B}}_{12} \circ \mathbb{D}_x) \\
K_{32} &= \mathbb{D}xx(\boldsymbol{\mathcal{B}}_{12} \circ \mathbb{D}_y) + 2\mathbb{D}xy(\boldsymbol{\mathcal{B}}_{66} \circ \mathbb{D}_x) + \mathbb{D}yy(\boldsymbol{\mathcal{B}}_{22} \circ \mathbb{D}_y) \\
K_{33} &= -\mathbb{D}xx\big((\boldsymbol{\mathcal{D}}_{11} \circ \mathbb{D}_{xx} + \boldsymbol{\mathcal{D}}_{12} \circ \mathbb{D}_{yy})\big) - 2\mathbb{D}xy(2\boldsymbol{\mathcal{D}}_{66} \circ \mathbb{D}_{xy}) \\
&\quad - \mathbb{D}yy\big((\boldsymbol{\mathcal{D}}_{12} \circ \mathbb{D}_{xx} + \boldsymbol{\mathcal{D}}_{22} \circ \mathbb{D}_{yy})\big) \\
&\quad + \big(K_p(\mathbb{D}xx + \mathbb{D}yy) - K_w\mathbb{I}\big) \\
K_{34} &= \mathbb{D}xx\big(-(\boldsymbol{\mathcal{D}}^s_{11} \circ \mathbb{D}_{xx} + \boldsymbol{\mathcal{D}}^s_{12} \circ \mathbb{D}_{yy})\big) - 2\mathbb{D}xy(2\boldsymbol{\mathcal{D}}^s_{66} \circ \mathbb{D}_{xy}) \\
&\quad - \mathbb{D}yy\big((\boldsymbol{\mathcal{D}}^s_{12} \circ \mathbb{D}_{xx} + \boldsymbol{\mathcal{D}}^s_{22} \circ \mathbb{D}_{yy})\big) \\
&\quad + \big(K_p(\mathbb{D}xx + \mathbb{D}yy) - K_w\mathbb{I}\big) \\
K_{41} &= \mathbb{D}xx(\boldsymbol{\mathcal{B}}^s_{11} \circ \mathbb{D}_x) + 2\mathbb{D}xy(\boldsymbol{\mathcal{B}}^s_{66} \circ \mathbb{D}_y) + \mathbb{D}yy(\boldsymbol{\mathcal{B}}^s_{12} \circ \mathbb{D}_x) \\
K_{42} &= \mathbb{D}xx(\boldsymbol{\mathcal{B}}^s_{12} \circ \mathbb{D}_y) + 2\mathbb{D}xy(\boldsymbol{\mathcal{B}}^s_{66} \circ \mathbb{D}_x) + \mathbb{D}yy(\boldsymbol{\mathcal{B}}^s_{22} \circ \mathbb{D}_y) \\
K_{43} &= -\mathbb{D}xx(\boldsymbol{\mathcal{D}}^s_{11} \circ \mathbb{D}_{xx} + \boldsymbol{\mathcal{D}}^s_{12} \circ \mathbb{D}_{yy}) - 2\mathbb{D}xy(2\boldsymbol{\mathcal{D}}^s_{66} \circ \mathbb{D}_{xy}) - \mathbb{D}yy\big((\boldsymbol{\mathcal{D}}^s_{12} \circ \\
&\mathbb{D}_{xx} + \boldsymbol{\mathcal{D}}^s_{22} \circ \mathbb{D}_{yy})\big) + \big(K_p(\mathbb{D}xx + \mathbb{D}yy) - K_w\mathbb{I}\big) \\
K_{44} &= -\mathbb{D}xx(\boldsymbol{\mathcal{H}}^s_{11} \circ \mathbb{D}_{xx} + \boldsymbol{\mathcal{H}}^s_{12} \circ \mathbb{D}_{yy}) - 2\mathbb{D}xy(2\boldsymbol{\mathcal{H}}^s_{66} \circ \mathbb{D}_{xy}) \\
&\quad - \mathbb{D}yy(\boldsymbol{\mathcal{H}}^s_{12} \circ \mathbb{D}_{xx} + \boldsymbol{\mathcal{H}}^s_{22} \circ \mathbb{D}_{yy}) + \mathbb{D}x(\boldsymbol{\mathcal{A}}^s_{55} \circ \mathbb{D}y) \\
&\quad + \mathbb{D}y(\boldsymbol{\mathcal{A}}^s_{44} \circ \mathbb{D}y) + \big(K_p(\mathbb{D}xx + \mathbb{D}yy) - K_w\mathbb{I}\big)
\end{aligned} \quad \textbf{(33)}$$

NUMERICAL RESULTS

This section presents the verification of the developed model with previous respectable published articles. After that, parametric studies will be considered to present the influence of gradation indices, slenderness ratio, and aspect ratio on natural frequencies of 2D-FG higher order shear deformation plate.

Validation

Table 1 presents the material properties of aluminum as a metal and Alumina as ceramic used in the validation section.

Table 1 Material properties of FGM plate

Material Property	Metal Aluminum (Al)	Ceramic Alumina (Al_2O_3)
$E(GPa)$	70	380
ν	0.3	0.3
$\rho(kg/m^3)$	2707	3800

Table 2 illustrates the validation of the present model with three previous works of Nguyen et al. [23], Matsunaga [24] and Thai and Choi [25] for FG plate with fully simple support boundary conditions. As seen for the small value of a/h and $n_x = 0$, the current result is identical with that obtained by Thai and Choi [25] and lies between the results obtained by Nguyen et al. [23], Matsunaga [24]. However, for large value of $a/h = 10$, all results are approximately identical. It is noted by increasing the gradation index through the thickness from 0 to 0.5, the natural frequency is decreased within 15%. By increasing the a/h from 2 to 5, the natural frequency decreased dramatically. It can conclude that, the effect of slenderness ration a/h has significant influence rather than the gradation index on the first natural frequency of FG plate.

Table 2 Comparison of the first non-dimensional frequencies $\bar{\omega} = \omega h\sqrt{\rho_c/E_c}$ of isotropic Al/Al_2O_3 SSSS square plates

$(h = 1, n_x = 0)$	a/h	n_z 0	0.5	1	4	10
Present	2	0.9297	0.8105	0.7356	0.5924	0.5414
Nguyen et al. [23]		0.9114	0.8099	0.7445	0.6165	0.5417
Matsunaga [24] Quasi-3D*		0.9400	0.8233	0.7477	0.5997	0.5460
Thai and Choi [25] S-FSDT**		0.9265	0.8062	0.7333	0.6116	0.5644
Present	5	0.2113	0.1806	0.1631	0.1378	0.1301
Nguyen et al. [23]		0.2100	0.1808	0.1639	0.1401	0.1304
Matsunaga [24] Quasi-3D*		0.2121	0.1819	0.1640	0.1383	0.1306
Thai and Choi [25] S-FSDT**		0.2112	0.1805	0.1631	0.1397	0.1324
Present	10	0.0577	0.0490	0.0442	0.0381	0.0364
Nguyen et al. [23]		0.0576	0.0490	0.0443	0.0383	0.0364
Matsunaga [24] Quasi-3D*		0.0578	0.0492	0.0443	0.0381	0.0364
Thai and Choi [25] S-FSDT**		0.0577	0.0490	0.0442	0.0382	0.0366

Table 3 Comparison of the first non-dimensional frequency $\bar{\omega} = \omega(a^2/h)\sqrt{\rho_c/E_c}$ of Al/Al_2O_3 square plates. $(a/h = 10, b = a = 1, n_x = 0.5)$

Boundary Conditions	n_z				
	0	0.5	1	2	5
CCCC	8.7434	7.6036	7.0121	6.5020	6.1229
SCSC	7.3291	6.3310	5.8208	5.3945	5.0999
CCCF	5.8552	5.1197	4.7431	4.4072	4.1877
CFCF	5.3757	4.6942	4.3482	4.0508	3.8397
SSSS	5.1175	4.4126	4.0579	3.7700	3.5866
SCSF	3.3329	2.8695	2.6379	2.4521	2.3389
SSSF	3.0791	2.6507	2.4364	2.2650	2.1613
SFSF	2.5709	2.2085	2.0274	1.8832	1.7969

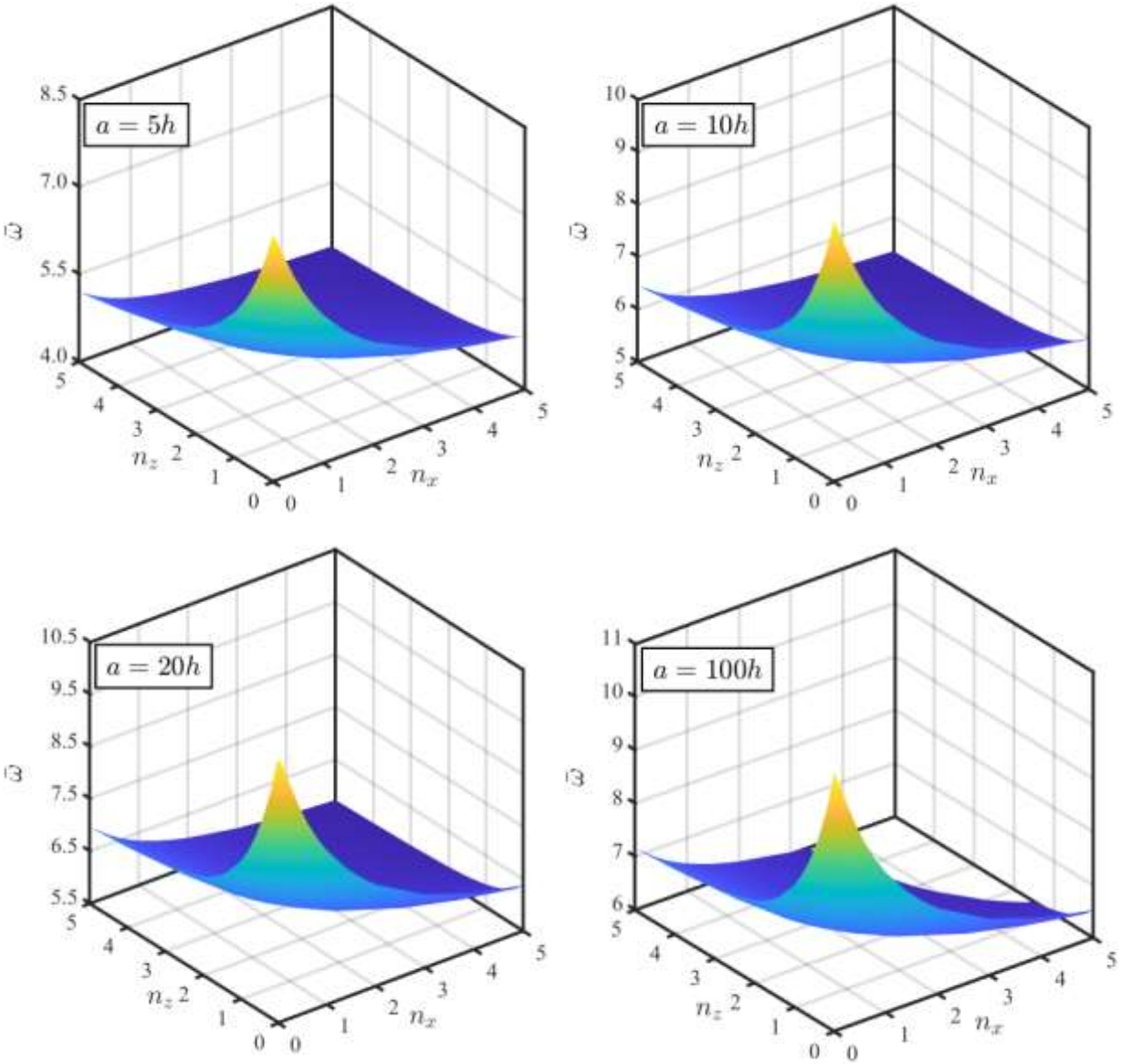

Figure 1 The effect of the gradient indices n_x and n_z on the dimensionless fundamental frequency $\bar{\omega} = \omega(a^2/h)\sqrt{\rho_c/E_c}$ of BDFG CCCC plate at a/h= 5,10,20 and 100.

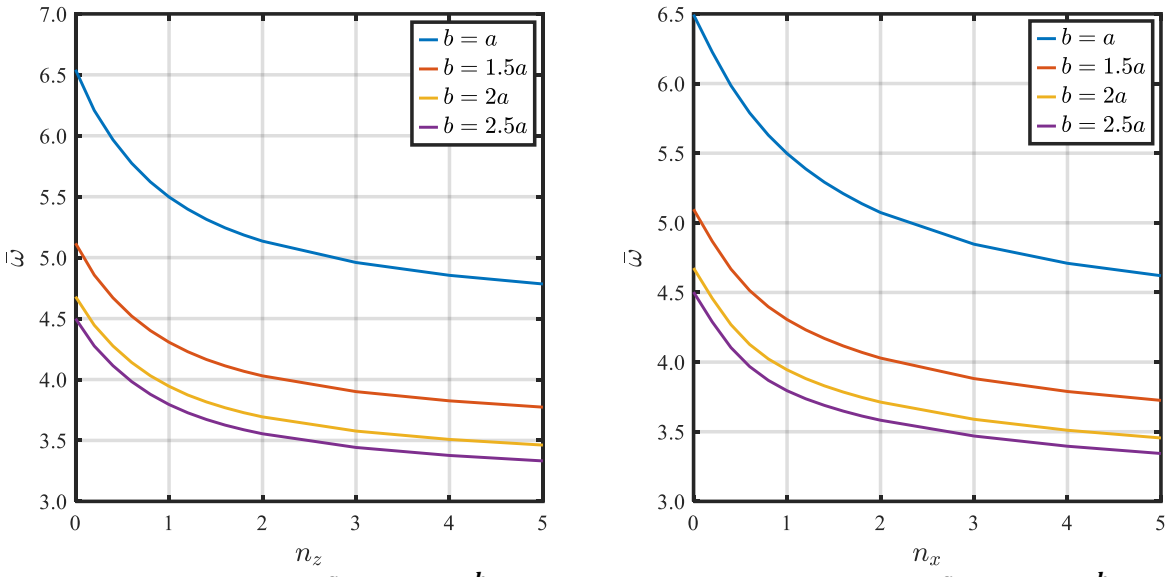

$\bar{\omega}$ versus n_z ($n_x = 1, \frac{a}{h} = 5$ and $\frac{b}{a} = 1, 1.5, 2, 2.5$)

$\bar{\omega}$ versus n_x ($n_z = 1, \frac{a}{h} = 5$ and $\frac{b}{a} = 1, 1.5, 2, 2.5$)

Figure 2 The effect of plate aspect ratio on the fundamental frequencies of 2D-FG plate with fully clamped boundary condition.

Parametric studies

The influence of gradation index though the thickness direction on the natural frequency of 2D-FG plate at different boundary conditions is presented in table 3. As noticed, by increasing the gradation index the material constituents will change from ceramics phase to metal phase, therefore, the stiffness of the plate structure will decrease and hence the natural frequency will decrease in the consequence. It is also observed that, the highest natural frequency is obtained in case of fully clamped boundary condition (CCCC) and the smallest natural frequency is acquired for simply-free-simply-free (SFSF) boundary condition, which is consistent with the physical explanation. It is found that, the natural frequencies for the clamped-clamped-clamped-free (CCCF), clamped-free-clamped-free (CFCF), and fully simply supported (SSSS) are very close.

The effect of gradation indices in axial and thickness direction on the first natural frequency of fully clamped 2D-FG plate at different slenderness ratio is portrayed in Figure 1. It is noted by increasing the gradation index in axial gradation and in thickness direction, the natural frequency decreased. As seen a curved shape is created due to the coupling effect of both gradation indices. However, increasing the ratio of a/h, the natural frequency is increased. For these cases, the highest natural frequency is noticed at $n_z = n_x = 0$ and a=100 h and the smallest natural frequencies is obtained at $n_z = n_x = 5$ and a=5h. It can be summarized that the gradation indices, slenderness ratio, and boundary conditions have the significant effects on the natural frequencies of 2D-FG Plate. Figure 2 presents the influence

of aspect ratio on the natural frequency of fully clamped 2D-FG plate. As concluded, by increasing the width/length ratio (b/a) the natural frequency is reduced. It noted that as the influence of aspect ratio on the frequency is decreased as the aspect ratio increased. This means that by increasing the aspect ratio from 1 to 1.5 the natural frequency is reduced by around 25%. However, by increasing the aspect ratio from 2 to 2.5, the natural frequency is reduced by around 5%.

CONCLUSIONS

The mathematical model solved by numerical differential integral quadrature method is proposed to investigate the free vibration of bidirectional functionally graded plate. Higher order shear deformation theory is used to describe the kinematic field and power law is used to grade the material constituent ceramic-metal phase through the axial and thickness direction. Hamilton's principle is exploited to derive the equations of motion and associated boundary conditions. The main points can be drawn from this model as follow:

1. By increasing the gradation index the material constituents will change from ceramics phase to metal phase, therefore, the stiffness of the plate structure will decrease and hence the natural frequency will decrease.

2. By increasing the gradation index in axial gradation and in thickness direction, the natural frequency decreased.

3. The highest natural frequency is obtained in case of CCCC, and the smallest natural frequency is acquired for SFSF boundary conditions.

4. The natural frequencies for CCCF, CFCF, and SSSS are very close.

5. By increasing the width/length ratio (b/a) the natural frequency is reduced.

REFERENCES

1. **Alshorbagy, A. E., Eltaher, M. A., & Mahmoud, F. "Free vibration characteristics of a functionally graded beam by finite element method", Applied Mathematical Modelling, 35(1), pp. 412-425, 2011.**
2. **Esen, I., Özarpa, C., & Eltaher, M. A. "Free vibration of a cracked FG microbeam embedded in an elastic matrix and exposed to magnetic field in a thermal environment", Composite Structures, 261, 113552. 2021.**
3. **Wu, C. P., & Huang, H. Y. A semianalytical finite element method for stress and deformation analyses of bi-directional functionally graded truncated conical shells. Mechanics Based Design of Structures and Machines, 48(4), pp. 433-458. 2020.**
4. **Abo-Bakr, H. M., Abo-Bakr, R. M., Mohamed, S. A., & Eltaher, M. A. Weight optimization of axially functionally graded microbeams under buckling and vibration behaviors. Mechanics Based Design of Structures and Machines, pp. 1-22. 2020.**
5. **Abo-Bakr, H. M., Abo-bakr, R. M., Mohamed, S. A., & Eltaher, M. A.. Multi-objective shape optimization for axially functionally graded microbeams. Composite Structures, 258, 113370, 2021.**
6. **Yu, T., Yin, S., Bui, T. Q., Xia, S., Tanaka, S., & Hirose, S. NURBS-based isogeometric analysis of buckling and free vibration problems for laminated composites plates with complicated cutouts using a new simple FSDT theory and level set method. Thin-Walled Structures, 101, pp. 141-156. 2016.**

7. **Nguyen, H. N., Hong, T. T., Vinh, P. V., Quang, N. D., & Thom, D. V. A refined simple first-order shear deformation theory for static bending and free vibration analysis of advanced composite plates. Materials, 12(15), 2385. 2019.**

8. **Khiloun, M., Bousahla, A. A., Kaci, A., Bessaim, A., Tounsi, A., & Mahmoud, S. R. Analytical modeling of bending and vibration of thick advanced composite plates using a four-variable quasi 3D HSDT. Engineering with Computers, 36(3), pp. 807-821, 2020**

9. **Arshid, E., Khorasani, M., Soleimani-Javid, Z., Amir, S., & Tounsi, A. Porosity-dependent vibration analysis of FG microplates embedded by polymeric nanocomposite patches considering hygrothermal effect via an innovative plate theory. Engineering with Computers, pp. 1-22, 2021.**

10. **Pham, Q. H., Tran, V. K., Tran, T. T., Nguyen-Thoi, T., & Nguyen, P. C. A nonlocal quasi-3D theory for thermal free vibration analysis of functionally graded material nanoplates resting on elastic foundation. Case Studies in Thermal Engineering, 26, 101170, 2021.**

11. **Attia, M. A., & Shanab, R. A. Vibration characteristics of two-dimensional FGM nanobeams with couple stress and surface energy under general boundary conditions. Aerospace Science and Technology, 111, 106552, 2021.**

12. **Shanab, R. A., & Attia, M. A. On bending, buckling and free vibration analysis of 2D-FG tapered Timoshenko nanobeams based on modified couple stress and surface energy theories. Waves in Random and Complex Media, pp. 1-47, 2021.**

13. **Hendi, A. A., Eltaher, M. A., Mohamed, S. A., Attia, M. A., & Abdalla, A. W. Nonlinear thermal vibration of pre/post-buckled two-dimensional FGM tapered microbeams based on a higher order shear deformation theory. Steel and Composite Structures, 41(6), pp. 787-802, 2021.**

14. **Ohab-Yazdi, S. M. K., & Kadkhodayan, M. Free vibration of bi-directional functionally graded imperfect nanobeams under rotational velocity. Aerospace Science and Technology, 119, 107210, 2021.**

15. **Van Vinh, P. Deflections, stresses and free vibration analysis of bi-functionally graded sandwich plates resting on Pasternak's elastic foundations via a hybrid quasi-3D theory. Mechanics Based Design of Structures and Machines, 1-32, 2021.**

16. **Sadgui, A., & Tati, A. A novel trigonometric shear deformation theory for the buckling and free vibration analysis of functionally graded plates. Mechanics of Advanced Materials and Structures, pp. 1-16, 2021.**

17. **Tran, T. T., Nguyen, P. C., & Pham, Q. H. Vibration analysis of FGM plates in thermal environment resting on elastic foundation using ES-MITC3 element and prediction of ANN. Case Studies in Thermal Engineering, 24, 100852, 2021.**

18. **Civalek, Ö., & Avcar, M. Free vibration and buckling analyses of CNT reinforced laminated non-rectangular plates by discrete singular convolution method. Engineering with Computers, 38, pp. 489–521, 2022.**

19. **Barati, A., Hadi, A., Nejad, M. Z., & Noroozi, R. On vibration of bi-directional functionally graded nanobeams under magnetic field. Mechanics Based Design of Structures and Machines, 50(2), 468-485, 2022.**

20. **Babaei, M., Asemi, K., & Kiarasi, F. Static response and free-vibration analysis of a functionally graded annular elliptical sector plate made of saturated porous material based on 3D finite element method. Mechanics Based Design of Structures and Machines, pp. 1-25, 2020.**

21. **Katiyar, V., & Gupta, A. Vibration response of a geometrically discontinuous bi-directional functionally graded plate resting on elastic foundations in thermal environment with initial imperfections. Mechanics Based Design of Structures and Machines, pp. 1-29, 2021.**

22. **Sah, S. K., & Ghosh, A. Influence of porosity distribution on free vibration and buckling analysis of multi-directional functionally graded sandwich plates. Composite Structures, 279, 114795, 2022.**

23. **Nguyen-Xuan, H., Tran, L. V., Thai, C. H., & Nguyen-Thoi, T. Analysis of functionally graded plates by an efficient finite element method with node-based strain smoothing. Thin-Walled Structures, 54, pp. 1-18, 2012.**

24. **Matsunaga, H. Free vibration and stability of functionally graded plates according to a 2-D higher-order deformation theory. Composite structures, 82(4), pp. 499-512, 2008.**

25. **Thai, H. T., & Choi, D. H. A simple first-order shear deformation theory for the bending and free vibration analysis of functionally graded plates. Composite Structures, 101, pp. 332-340, 2013.**